



Enhancing high cycle stability of Ni-rich $\text{LiNi}_{0.94}\text{Co}_{0.04}\text{Al}_{0.02}\text{O}_2$ layered cathode material

Wei Liu^{1,2} · Xu Cheng² · Chao Wang¹ · Bingbing Zhao³ · Bingxin Huang²

Received: 29 July 2021 / Revised: 14 August 2021 / Accepted: 16 August 2021 / Published online: 23 August 2021
© The Author(s), under exclusive licence to Springer-Verlag GmbH Germany, part of Springer Nature 2021

Abstract

The layered lattice structure of the nickel-rich $\text{LiNi}_{0.94}\text{Co}_{0.04}\text{Al}_{0.02}\text{O}_2$ (NCA) cathode material has the advantages of high energy density and low cost. Unfortunately, high nickel materials' application is limited due to the fast decay of capacity. Doping and coating are effective methods to enhance cycle stability. In this study, the effects of Ti doping on the electrochemical performances of NCA are systematically investigated. $\text{Ni}_{0.94}\text{Co}_{0.04}\text{Al}_{0.02}(\text{OH})_2$ and TiO_2 are directly mixed, and after sintering, Ti^{4+} ions diffused uniformly in the $\text{LiNi}_{0.94}\text{Co}_{0.04}\text{Al}_{0.02}\text{O}_2$ cathode particles. Besides, $(\text{Ni}_{0.4}\text{Co}_{0.2}\text{Mn}_{0.4})_{0.78}\text{Ti}_{0.22}(\text{OH})_2$ is coated onto the surface of $\text{Ni}_{0.94}\text{Co}_{0.04}\text{Al}_{0.02}(\text{OH})_2$ precursor particles with a facile co-precipitation method, and after sintering, Ti^{4+} ions also diffused uniformly. The cathodes were cycled in the voltage range of 2.8–4.5 V at 1 C. As a result, the discharge capacity of $\text{Ni}_{0.94}\text{Co}_{0.04}\text{Al}_{0.02}(\text{OH})_2$ changes from 201.4 to 119.8 mAh g^{-1} , and the battery capacity decayed rapidly within 200 cycles. Although the initial discharge capacity of the doped and covered specimens was not significantly dissimilar from the original precursor specimens, the capacity has only dropped by 20% after 200 charges and discharges.

Keywords Nickel-rich NCA · Ti-doping · Coating · Capacity

Introduction

Global warming is a worldwide issue that requires improvement of energy efficiency and reduction of CO_2 emission. Environmental friendly electronic equipment and new energy vehicles are increasingly used daily [1, 2]. As lithium-ion batteries produce effective power for the engine, the mileage that lithium batteries can provide to electric vehicles is critical to market competitiveness. It needs to develop lithium-ion batteries with good cycle stability and a large operating temperature range [3]. One crucial factor in

determining the performance of rechargeable batteries is the cathode material [4, 5], among which the layered nickel-rich cathode materials such as LiNiCoAlO_2 and LiNiCoMnO_2 attract the most attention due to their high specific capacity [6–8].

The severe capacity degradation of LiNiCoAlO_2 still hinders its commercialization [9]. In recent years, there are numerous reports promoting battery capacity retention rates by doping Mg, Ti, La, Zr, Nb, etc. These elements play a certain in enhancing the cycle performance of electrodes and demonstrate different impacts. The similar ionic radius of Mg^{2+} and Li^+ allows Mg^{2+} to occupy Li^+ sites preferentially and reduce cation mixing [10]. Ti doping can fruitfully impede the structural degradation of the cathode electrode particles. Doping can also reduce the side reaction of the electrolyte and more interfaces [11, 12].

In recent years, high nickel ($\geq 90\%$) materials with extremely high specific capacity are appearing [13–15]. In this study, a layer of dense precipitate was formed on the exterior of $\text{Ni}_{0.94}\text{Co}_{0.04}\text{Al}_{0.02}(\text{OH})_2$ precursor particles by the co-precipitation method. Meanwhile, the cathode material is formed by physically doping different proportions of nano- TiO_2 particles, mixed with lithium and sintered. The increased cycle stability of high nickel materials was

✉ Chao Wang
c.wang@cqu.edu.cn

✉ Bingbing Zhao
zhao.bb@sjtu.edu.cn

✉ Bingxin Huang
bxhuang@ustb.edu.cn

¹ College of Mechanical and Vehicle Engineering, Chongqing University, Chongqing 400030, China

² Shunde Graduate School of University of Science and Technology Beijing, Foshan 528399, China

³ School of Materials Science and Engineering, Shanghai Jiao Tong University, Shanghai 200240, China

analyzed by various characterization techniques to explore the correlation between the electrochemical properties and the microstructure.

Materials and methods

The precursor $\text{Ni}_{0.94}\text{Co}_{0.04}\text{Al}_{0.02}(\text{OH})_2$ is a commercial material (Zhejiang Province, China). $\text{Ni}_{0.94}\text{Co}_{0.04}\text{Al}_{0.02}(\text{OH})_2$ and TiO_2 nanoparticles were fully mixed in an agate mortar and then blended with lithium. The powder was sintered into the cathode materials $\text{Li}(\text{Ni}_{0.94}\text{Co}_{0.04}\text{Al}_{0.02})_{1-x}\text{Ti}_x\text{O}_2$ ($x=0.008, 0.01, 0.012, 0.015$), which were named as NCA-Ti0.8%, NCA-Ti1.0%, NCA-Ti1.2%, and NCA-Ti1.5%, respectively. Based on the composition of the coating layer, $\text{NiSO}_4 \cdot 6\text{H}_2\text{O}$, $\text{CoSO}_4 \cdot 7\text{H}_2\text{O}$, $\text{MnSO}_4 \cdot \text{H}_2\text{O}$, and $\text{Ti}(\text{SO}_4)_2$ were weighted to form a 0.5 mol/L metal salt solution. The pH value of the liquor was modified to 3 by HCl acid due to the existence of Ti^{4+} . The obtained metal salt solution was slowly dripped into the deionized aqueous solution of $\text{Ni}_{0.94}\text{Co}_{0.04}\text{Al}_{0.02}(\text{OH})_2$ by a peristaltic pump. The pH value of the liquor was controlled between 10.5 and 10.8 by dripping ammonia water. The resulting mixed solution was rinsed with deionized water 3 times to clean up excessive impurity ions. Then, the washed precipitate was baked in a vacuum drying oven for 12 h to acquire the $\text{Ni}_{0.94}\text{Co}_{0.04}\text{Al}_{0.02}(\text{OH})_2$ precursor after coating of $(\text{Ni}_{0.4}\text{Co}_{0.2}\text{Mn}_{0.4})_{0.78}\text{Ti}_{0.22}(\text{OH})_2$. The coated precursor was mixed with lithium and sintered to a cathode material named as NCA-NCM424Ti. An excess of 6% $\text{LiOH} \cdot \text{H}_2\text{O}$ was subjoined to reimburse the Li deficiency during high-temperature sintering. The compound was preheated in a tube furnace in pure oxygen at 500 °C for 2 h, and then calcined at 710 °C for 14 h. The electrochemical inert material TiO_2 is used to reduce the contact between the surface of the material and the electrolyte, and reduce the side reaction with the electrolyte. The use of the co-precipitation method to form a core-shell structure with

high nickel ($\text{Li}(\text{Ni}_{0.94}\text{Co}_{0.04}\text{Al}_{0.02})\text{O}_2$) as the core and low nickel ($\text{Li}(\text{Mn}_{0.4}\text{Co}_{0.2}\text{Ni}_{0.4})_{0.78}\text{Ti}_{0.22}\text{O}_2$) as the outer shell has a stable surface structure.

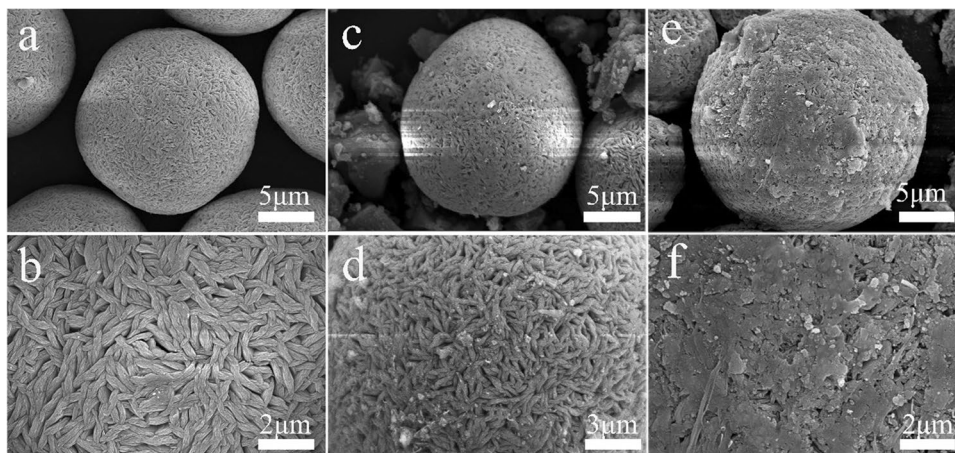
The loading amount of the active material in the electrode was 3–3.5 mg cm^{-2} . The mass ratio of the three components, i.e., active materials, acetylene black (conductive agents) and polyvinylidene (PVDF, binder), in the cathode material is 8:1:1. The cathode materials were assembled into a button battery (CR2032) in the glove box. The cathode material and the anode lithium sheet were divided by a microporous membrane (Celgard 2300). The current was set as 0.1 C for the earliest 4 cycles to actuate the batteries, and then increased to 1 C in the later cycles. To measure the magnification effect, the battery was cycled 5 times at 0.1 C, 0.2 C, 0.5 C, 1 C, 2 C, and 5 C at a voltage of 2.8–4.5 V, respectively. Electrochemical impedance spectroscopy (EIS) and cyclic voltammetry (CV) curves were generated using an electrochemical workstation (PGSTAT302N, AUTOLAB) in the frequency range of 10^{-2} – 10^5 Hz.

We used scanning electron microscope (SEM; FEI Quanta 250 FEG) to reveal the morphology and composition of cathode particles. The surface elements and valence states were analyzed by X-ray photoelectron spectroscopy (XPS). The crystal structure of the particles was identified by powder X-ray diffraction (XRD) of Cu-K α radiation.

Results and discussion

The morphology of the three precursors was illustrated in Fig. 1. The size of the NCA precursor is 10–15 μm . The round and equiaxed NCA precursor (Fig. 1a) are constituted of needle-like primary particles, whose irregularity renders micro-pores in the NCA precursor (Fig. 1b). In comparison, the surface of the NCA-NCM424Ti precursor is covered by a thin shell, which is formed by stacking sheet hydroxides and hardly changes the size of the precursor. The micro-pores

Fig. 1 SEM of the particle, (a, b) NCA precursor, (c, d) NCA-Ti1.0% precursor, and (e, f) NCA-NCM424Ti precursor



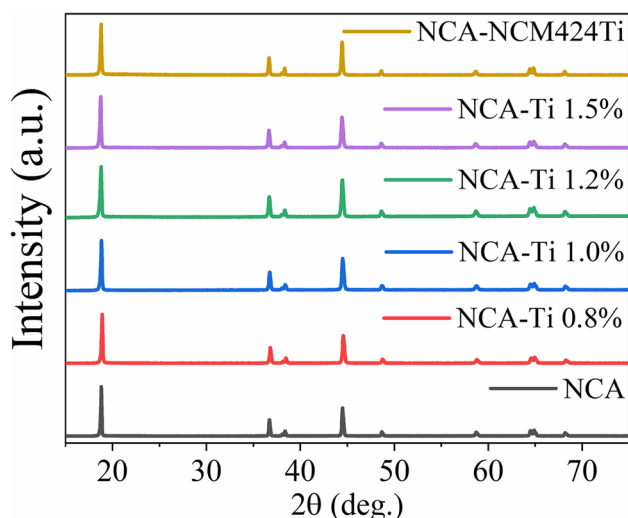


Fig. 2 XRD patterns of specimens

Table 1 The composition of different Ti-doped specimens was measured by EDS

	Ni (%)	Co (%)	Al (%)	Ti (%)
NCA	94.00	4.00	2.00	0.00
NCA-Ti0.8%	93.30	3.89	1.97	0.84
NCA-Ti1.0%	93.22	3.76	1.95	1.07
NCA-Ti1.2%	93.08	3.73	1.92	1.27
NCA-Ti1.5%	92.86	3.69	1.91	1.54

between the primary needle-like particles are diminished (Fig. 1e, f). The precursor of NCA-Ti1.0% demonstrates mediate needle-like crystal grains (Fig. 1c, d), which are apparently different from NCA-NCM424Ti due to the different experimental methods. When the micro-pores between the particles are small, the electrolyte is difficult to penetrate the interior of the precursor, and it reduces the damage to the particles. The composition of different Ti-doped samples was measured by EDS (Table 1). The prepared samples are basically consistent with the theoretical data. Researchers have developed various methods to modify NCA with metal elements. In particular, SiO₂ and TiO₂ nanoparticles are used to make dry coatings to stabilize the external of the

nanoparticles [16–18]. But in this article, TiO₂ is applied to directly dope on the exterior of the precursor. Many other materials can modify the structure of the surface layer of the positive electrode material, such as the use of ZrO₂ coating to enhance the Ni titanium oxide and thermal stability on the surface of the positive electrode material [19]. In addition, Co₃O₄ is used to coat the NCA cathode material to reduce the charge transfer resistance and increase the capacity retention rate [20]. Based on the above experimental methods, it is an effective way to enhance the durability of the battery by doping with metal or non-metal oxide.

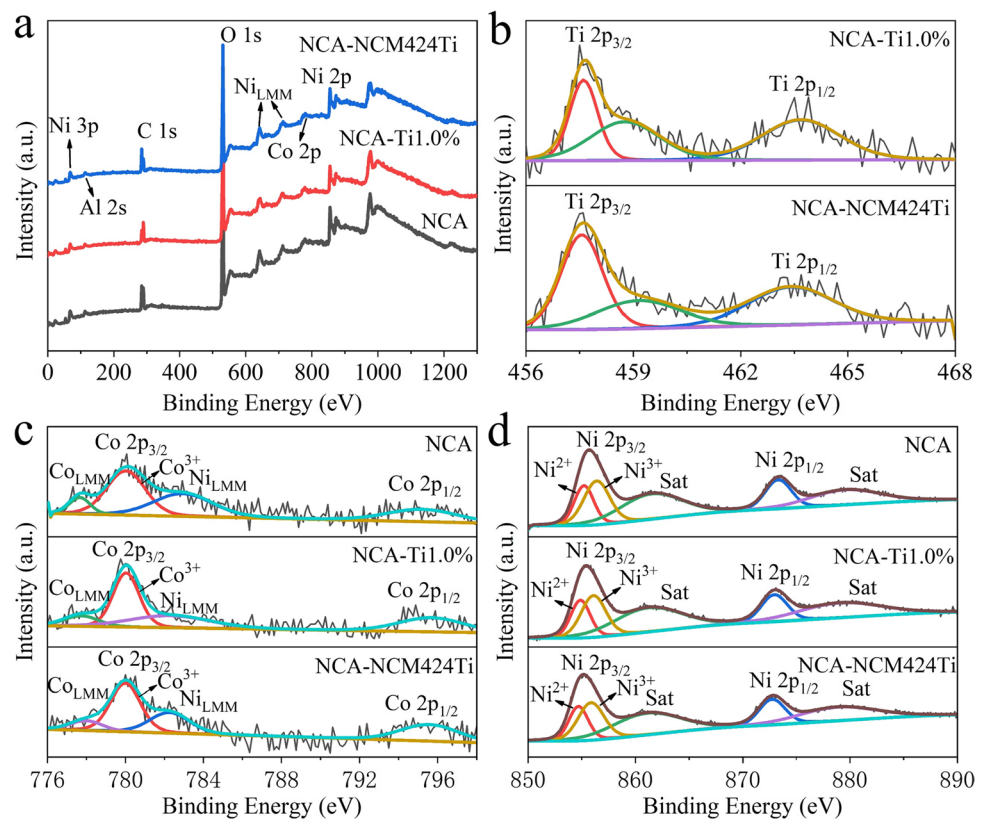
Figure 2 presents the XRD patterns of NCA, NCA-Ti0.8%, NCA-Ti1.0%, NCA-Ti1.2%, NCA-Ti1.5%, and NCA-NCM424Ti. All patterns obtained in the experiment are a layered α-NaFeO₂ type lattice structure [21–23]. There is no detected impurity phase. It reveals that the infiltration of elements will not change the original layered lattice structure [16, 24]. The ordered layered structure is demonstrated by the obvious splits of (006)/(102) and (018)/(110) peaks [10, 16, 24]. The intensity ratio of peaks I₍₀₀₃₎ and I₍₁₀₄₎ reflects the degree of cation mixing, i.e., a higher I₍₀₀₃₎/I₍₁₀₄₎ indicates that cation disturbances are reduced [22, 25]. When I₍₀₀₃₎/I₍₁₀₄₎ is < 1.2, the electrochemical performance deteriorates. When I₍₀₀₃₎/I₍₁₀₄₎ is > 1.5, the material has a complete lattice structure. The I₍₀₀₃₎/I₍₁₀₄₎ and lattice constants of the materials were classified in Table 2. NCA has the smallest I₍₀₀₃₎/I₍₁₀₄₎ ratio of 1.5499, while NCA-Ti 1.0% bears the highest value of 1.6916. It confirms that doping an appropriate amount of Ti can reduce cation mixing. The unit cell c/a values of the specimens are all greater than 4.9, which further demonstrates that the layered framework of the synthesized specimen is intact and orderly.

The electronic state of NCA, NCA-Ti1.0%, and NCA-NCM424Ti specimens were analyzed by XPS to study the change of valence state of Ni, Co, Al, and Ti on the exterior of the material. Figure 3a displays the Ni, Co, and Al oxidation state crests in NCA, NCA-Ti1.0%, and NCA-NCM424Ti specimens. Figure 3b shows that the micropores between the needle-like particles are filled with Ti elements through the coating and doping scheme. However, there are slight differences in the binding energies measured by the two experiments. The binding energies of the Ti 2p_{3/2} and 2p_{1/2} crests of NCA-NCM424Ti are 457.56 eV and 463.68 eV,

Table 2 Lattice parameters of specimens

Specimen	a/(Å)	c/(Å)	c/a	I ₍₀₀₃₎ /I ₍₁₀₄₎
NCA	2.8713(0.00003)	14.1815(0.0002)	4.9391	1.5499
NCA-Ti0.8%	2.8715(0.00006)	14.1816(0.0004)	4.9387	1.6179
NCA-Ti1.0%	2.8715(0.00004)	14.1861(0.0003)	4.9403	1.6916
NCA-Ti1.2%	2.8721(0.00005)	14.1943(0.0004)	4.9421	1.5818
NCA-Ti1.5%	2.8727(0.00005)	14.1978(0.0003)	4.9423	1.5768
NCA-NCM424Ti	2.8667(0.00004)	14.1706(0.0003)	4.9432	1.5501

Fig. 3 **a** XPS spectra, **b** Ti 2p spectra, **c** Co 2p spectra, and **d** Ni 2p spectra



which are only 0.05 eV and 0.25 eV lower than those of NCA-Ti1.0%, respectively. Moreover, the Ti 2p_{3/2} crest in the NCA-Ti1.0% specimen is sharper than NCA-NCM424Ti. It implies that there might be more titanium impurities on the exterior of the NCA-Ti1.0% specimen. The binding energy of the prominent crest of Co 2p_{3/2} (Co³⁺) is 778.00 eV. The Co 2p_{3/2} prominent crest is escorted by a Co(LMM) crest at 777.99 eV and a Ni(LMM) crest at 782.26 eV. Figure 3c illustrates that Co 2p_{1/2}'s binding energy is 795.57 eV. The Ni 2p XPS spectrum (Fig. 3d) is relatively complex. The Ni 2p_{1/2} crest at 872.73 eV has a satellite crest at 878.89 eV. The Ni 2p_{3/2} spectrum with one satellite crest (861.07 eV) has two other crests located at 854.70 eV and 855.87 eV, matching to Ni²⁺ and Ni³⁺, separately. Furthermore, the content of Ni²⁺ accounts for 40.37%. The stability of the particle structure is related to the Ni²⁺ ion on the surface of the particle [26, 27].

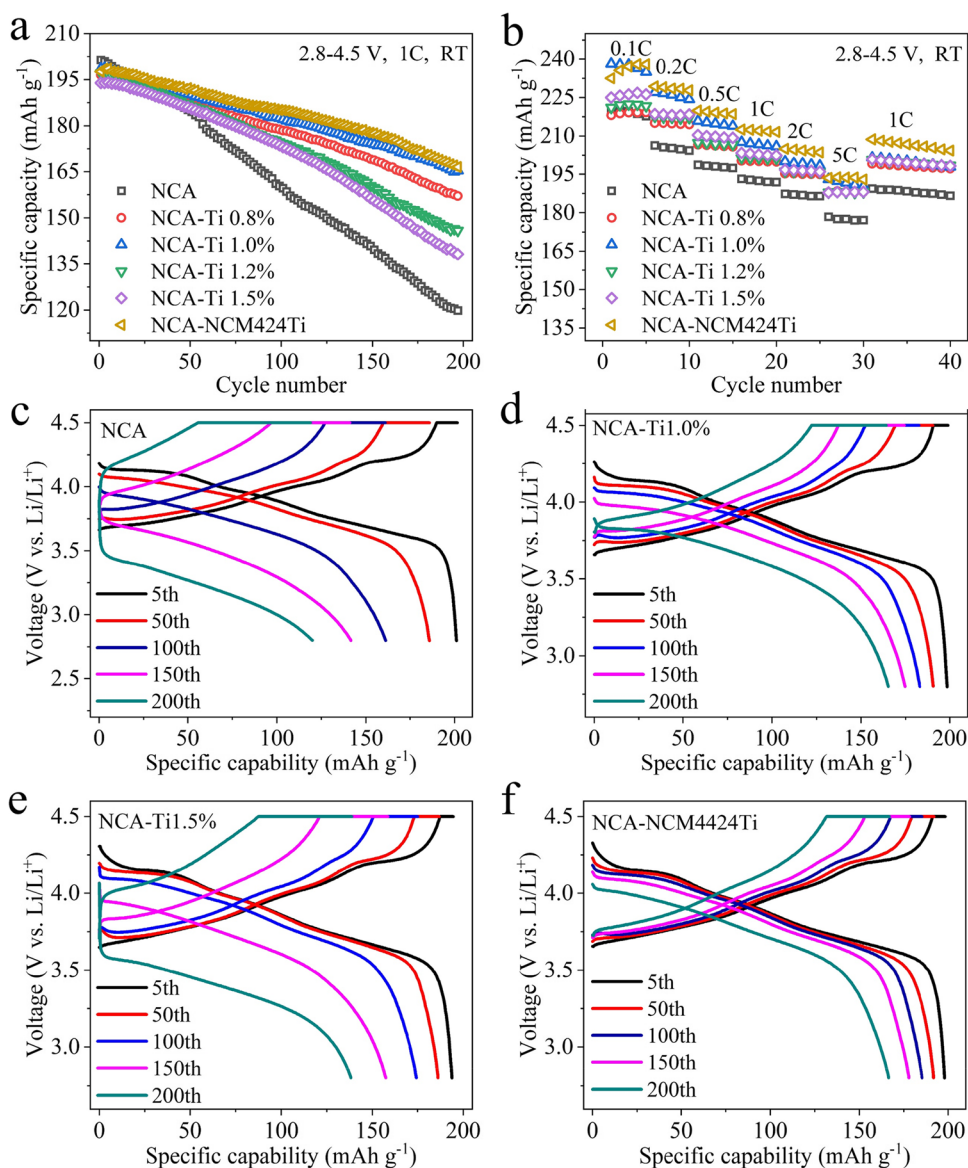
The capacity retention rate presents the electrochemical durability of a lithium battery. The cycle stability charge and discharge curves of the lithium battery in this work all have experienced 200 cycles. Figure 4a shows that the specific discharge capacity of NCA has dropped by 40%, from 201.4 to 119.8 mAh/g. Similarly, under the current state of 1 C, the discharge specific capacity of the first turn of modified battery is 1% lower than that of the unmodified battery. However, the capacity retention rate of NCA-NCM424Ti after the modification has been remarkably

enhanced. The discharge specific capacity of NCA-Ti1.0% decreases since 198.5mAh/g in the first round to 165.3 mAh/g, and the capacity preservation reached 83.27%. The highest capacity preservation of NCA-NCM424Ti is 83.68%. Its lithium battery's capacity slightly increases from 197.6 to 198.5 mAh/g during the primary five cycles. The infiltration of the Mn element may cause a slight increase in the capacity of the coated modified battery in the first few cycles, then declines to 166.1 mAh/g after 200 cycles.

Figure 4b shows the rate performance of lithium batteries. The NCA-Ti1.0% and NCM424Ti can deliver a higher specific discharge capacity while maintaining stable battery charge and discharge under different currents. The capacity of NCA-NAM424Ti is recovered to 208.7 mAh/g when the current is changed from a high rate to a low rate. This shows that both NCA doped with TiO₂ or NCA coated with NCM424Ti can increase the ion/electron conductivity of the material.

The polarization of batteries is a common phenomenon in nickel-rich cathode materials. Battery charging is divided into constant current charging and constant voltage charging. The charging and discharging curves (Fig. 4c–f) display that the time of the former increases and the time corresponding to the latter decreases after modified. It makes the extraction and insertion of Li⁺ easier compared to original NCA

Fig. 4 **a** Cycle performance of dissimilar specimens 200 times charge–discharge, **b** rate performance of dissimilar specimens 200 times charge–discharge, **c** charge–discharge curves of pure NCA specimen with dissimilar turns, **d** charge–discharge curves of NCA-Ti1.0% specimen with dissimilar turns, **e** charge–discharge curves of NCA-Ti1.5% specimen with dissimilar turns, and **f** charge–discharge curves of NCA-NCM424Ti specimen with dissimilar turns



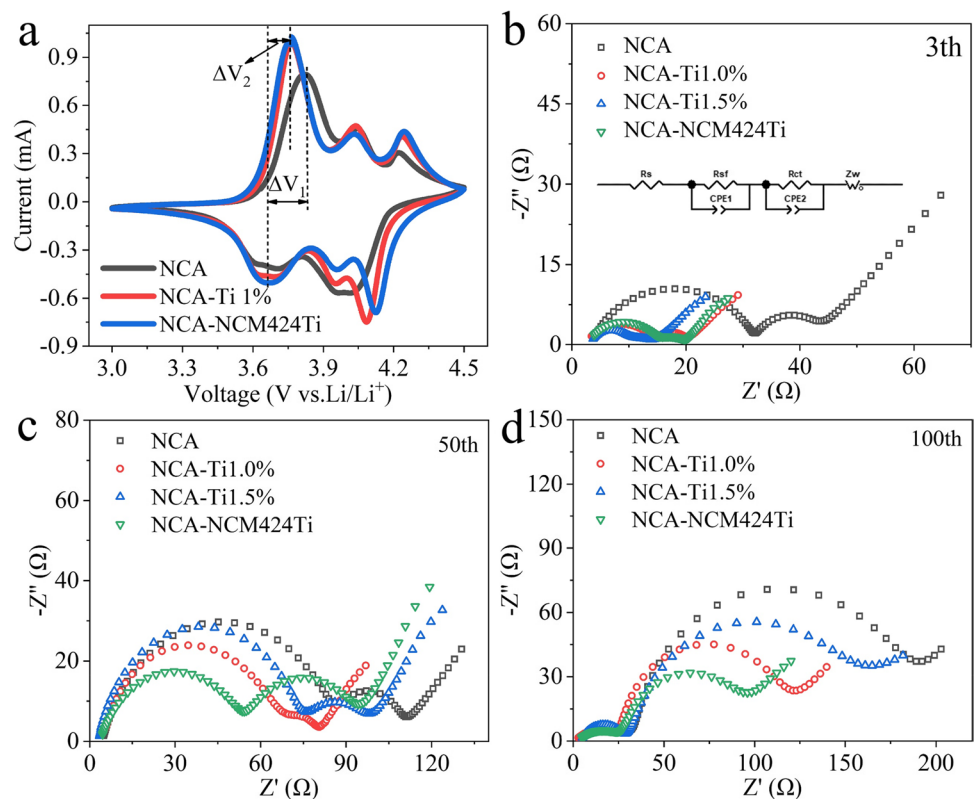
precursors. Therefore, the modification suppresses the voltage attenuation.

The cyclic voltammetry curve of the nickel-rich cathode material (Fig. 5a) shows three pronounced redox peaks, which correspond to the three phase transitions $H1 \rightarrow M$, $M \rightarrow H2$ and $H2 \rightarrow H3$, respectively [28, 29]. The extraction and intercalation of Li^+ mainly cause the reversibility of electrochemistry. The phase transition peak of the material is pronounced at ~ 3.7 V, where most intercalated lithium ions are released. The reversibility of electrochemistry is reflected by the redox potential difference (ΔV) between the oxidation peak and the reduction peak at the cyclic voltammetry curve [30, 31]. The voltage difference of NCA $\Delta V_1 = 0.107$ V means that the reversibility of Li^+ extraction and insertion of the original precursor is low. In contrast, the voltage difference between NCA-Ti1.0% and

NCA-NCM424Ti is $\Delta V_2 = 0.052$ V. Thus, the three peaks clearly indicate that the modification did not damage the original chemical reaction. The reduced ΔV value of the modified specimen accounts for the improvement of reversibility and decreased polarization.

The resistance of the cathode material correlates with the electrochemical evolution of the battery during cycling. The Nyquist diagram of the experimental specimens (Fig. 5b–d) usually consists of two arcs which represent the surface film resistance (R_{sf}) and charge transfer resistance (R_{ct}). The straight line in the curve is the Warburg resistance related to Li^+ diffusion in the positive electrode material [22, 25, 27, 32, 33]. In the current study, the EIS is measured at 4.0 V after 3, 50, and 100 cycles. The modified cathode material always maintains lower R_{sf} and R_{ct} than the original NCA precursor after 50 or 100 cycles. It is the evidence of

Fig. 5 **a** The CV plots of dissimilar specimens, **b** the Nyquist of dissimilar specimens after 3th cycle, **c** the Nyquist of dissimilar specimens after 50th cycle, and **d** the Nyquist of dissimilar specimens after 100th cycle



the stable interface and better cycle permanence [24]. The increase in R_{ct} could be correlated with the breakage of the particles and the mixing of cations. The relatively stable R_{sf} of the doped and covered cathode material is connected to the formation of a durable SEI film with higher conductivity. As Ti ions can reduce the mixed content of cations during charging and discharging, the modified cathode material displays better electrochemical performance.

The phase transition is represented by the cyclic voltammetry curve in Fig. 5a. The cyclic voltammetry curves (Fig. 6a–c) under different scan rates (0.1 mV s^{-1} , 0.2 mV s^{-1} , 0.3 mV s^{-1} , 0.4 mV s^{-1}) illustrate the kinetics of the electrode charging and discharging process. The Li^+ diffusion coefficient (D_{Li^+}) is a constant, which can be calculated by the scan rate v and the redox peak current (i_p) Randles–Sevcik formula [34, 35]:

$$i_p = 2.69 \times 10^5 n^{3/2} A D^{1/2} C_0 v^{1/2} \quad (1)$$

where n represents the amount of charge transfer in the redox process ($n=1$); A is the area occupied by the cathode material (cm^2); C_0 represents the number of reactants in the cathode material (mol cm^{-3}); $v^{1/2}$ is equal to the scan Speed (V s^{-1}). Figure 6d and e display the linear connection between the peak current of the charging and discharging process and the square root of $1/2$ times of the scan rate. From the Li^+ diffusion coefficient calculated in Table 3,

it can be summarized that the Li^+ diffusion coefficient of the specimen after doping modification has been noteworthy enhanced. During the reduction peak, the doping also improves the extraction and insertion of Li^+ .

Both the differential capacity voltage curve ($dQ/dV-V$) and the CV curve have three sets of redox peaks. The continuous three groups of redox peaks represent the continuous phase transition of H1-H2-H3 [36, 37]. The phase changes details of each circle are more visible in the $dQ/dV-V$ images. As evident in Fig. 7a, the button battery assembled from the original precursor has lost the adjustment ability from the M phase to the second hexagonal phase and then to the third hexagonal phase after 50 charge–discharge cycles. The lack of phase transformation leads to evident polarization, and the capacity cannot be fully utilized. Finally, the battery exhibits a rapid capacity decline, which is generated by the transform of the anisotropic lattice volume [38–41]. In contrast, the modified materials slow down the rate of particle rupture, and the structure can be retained.

Element mappings on the cross section of NCA-Ti1.0% and NCA-NCM424Ti particles are given in Fig. 8. Ni, Co, Al, Mn, and Ti are confirmed to exist in the particles. During the high-temperature sintering process, the new elements added through the modification are uniformly distributed into the particles. The uniform color mapping inside the particles shows that the coating and doping experiments make the micropores inside the modified particles smaller, which

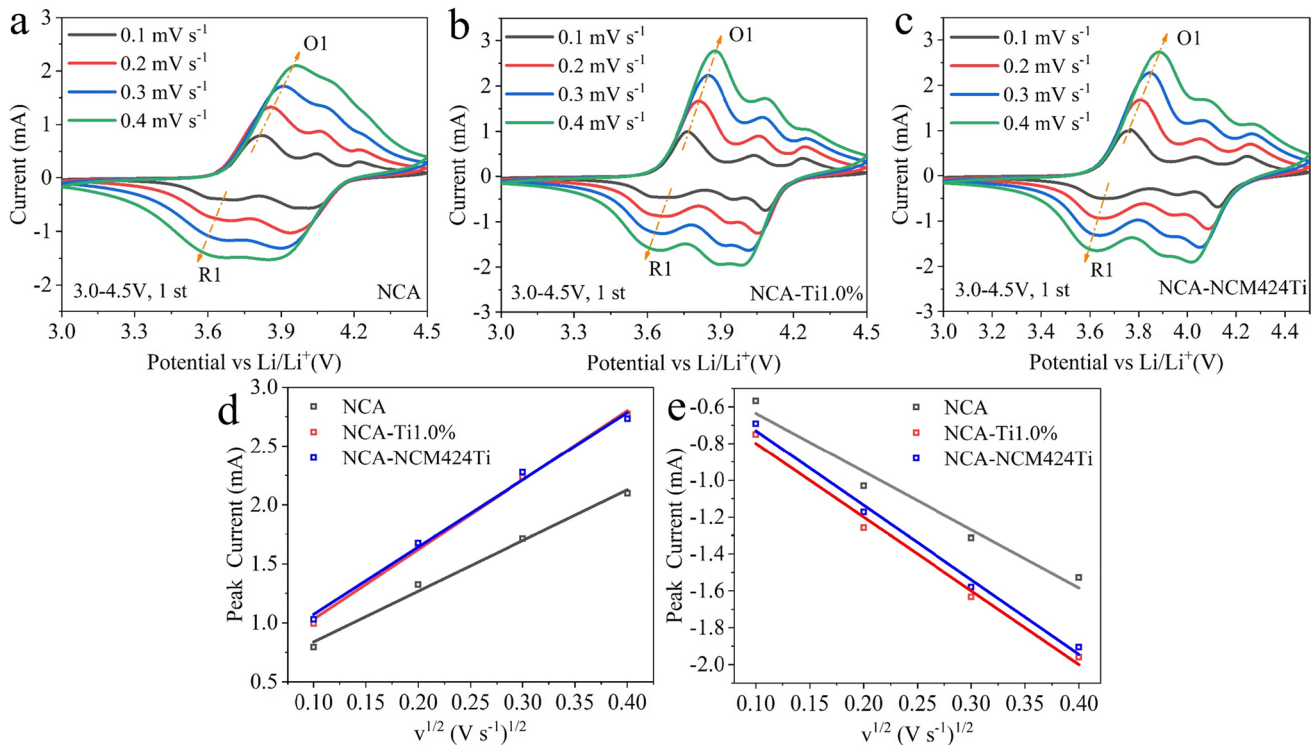


Fig. 6 CV curve at 0.1–0.4 mV s⁻¹ scan rates, (a) NCA specimen, (b) NCA-Ti1.0% specimen, (c) NCA-NCM424Ti specimen, (d) the linear relation between O1 peak currents and v^{1/2}, and (e) the linear relation between R1 peak currents and v^{1/2}

Table 3 Lithium ion diffusion coefficient of NCA specimen and modified specimen

	NCA	NCA-Ti1.0%	NCA-NCM424Ti
D _{OLi} ⁺ (cm ² s ⁻¹)	3.73 × 10 ⁻¹²	6.99 × 10 ⁻¹²	6.55 × 10 ⁻¹²
D _{RLi} ⁺ (cm ² s ⁻¹)	2.05 × 10 ⁻¹²	3.24 × 10 ⁻¹²	3.30 × 10 ⁻¹²

reduces the possibility of particles breaking and creating new interfaces in the process of lithium removal and lithium insertion in the battery. The side reactions between the electrolyte and the new interface are lessened [23, 25]. This also shows that the uniform surface coating and element doping strategy can be used as an industrially scalable method.

The morphologies of NCA, NCA-Ti1.0%, and NCA-NCM424Ti after 200 cycles (Fig. 9) were further characterized through SEM. After 200 cycles of NCA, it is challenging to observe complete spherical particles [42, 43]. On the contrary, complete spherical particles can still be observed in a large area after 200 cycles of NCA-Ti1.0% and NCA-NCM424Ti. There is no crack on the exterior. The electrochemical function of the high nickel cathode material NCA or NCM may have a specific relationship with the mechanical properties of the particles [44–46]. The extraction and embedding of Li⁺ is a cyclical process. The movement of Li⁺ reduces the mechanical properties of the particles and

increases the strain of the particles. Therefore, it is inevitable that NCA particles will crack during the cycle. When Li⁺ continues to escape from the embedding, the cracks of the particles will increase. The chance of the electrolyte coming into contact with the new interface continues to increase, which creates a phenomenon that continues to deteriorate. When the original precursor circulates to 200 cycles, there are no complete spherical particles (Fig. 9d) to support the charge and discharge of the battery. Therefore, the discharge specific capacity of the original precursor plummeted. Through Ti doping and NCM424Ti coating, the micropores between the secondary needle-shaped particles can be reduced, and the degree of side reaction between the new interface and the electrolyte can be reduced. The integrity of the particles is retained [45]. Therefore, the cycle durability of NCA-Ti1.0% and NCA-NCM424Ti can be significantly boosted.

Conclusion

For all measurements, the battery was tested at room temperature environment between 2.8 and 4.5 V and a current of 1 C. The capacity retention rate of NCA is only 59.48%. The NCA cathode material was modified through the doping experiment, and the electrochemical performance of

Fig. 7 dQ/dV outline of specimens, **(a)** NCA, **(b)** NCA-Ti1.0%, **(c)** NCA-Ti1.5%, and **(d)** NCA-NCM424Ti

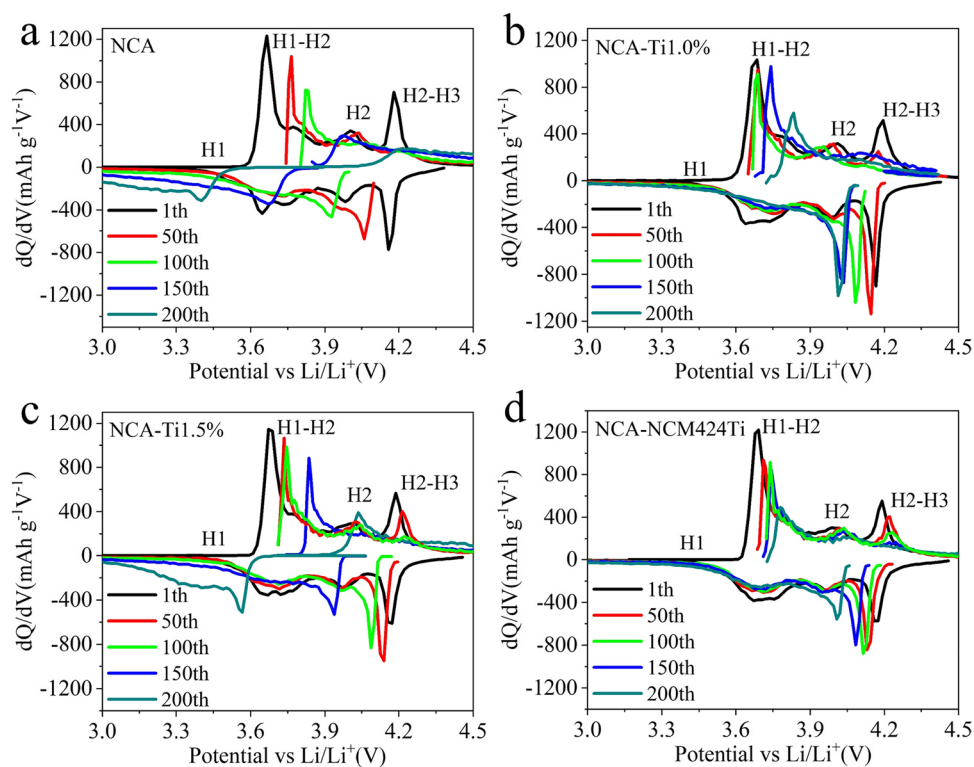
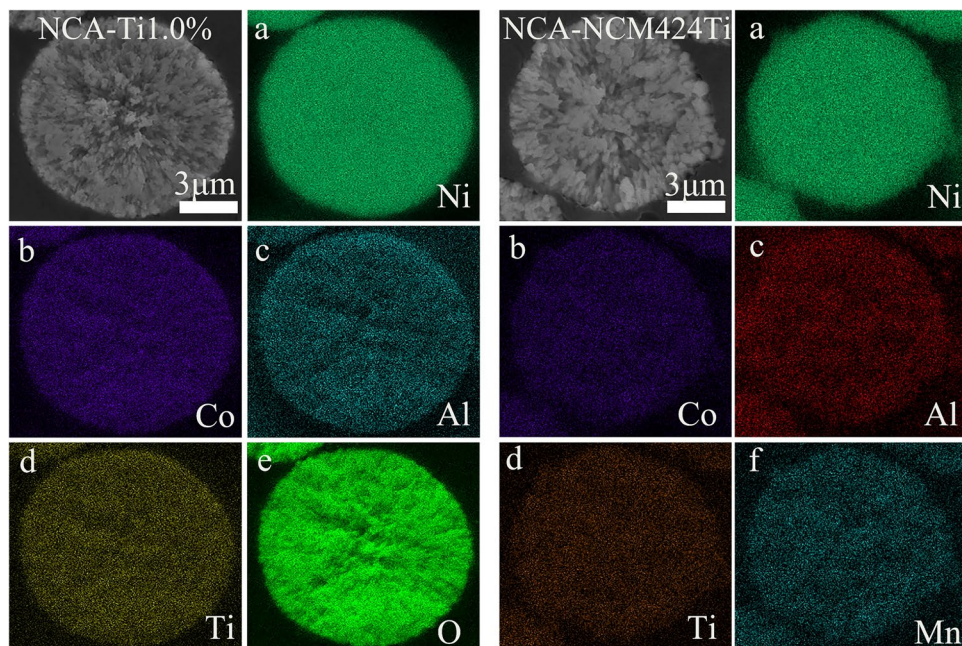


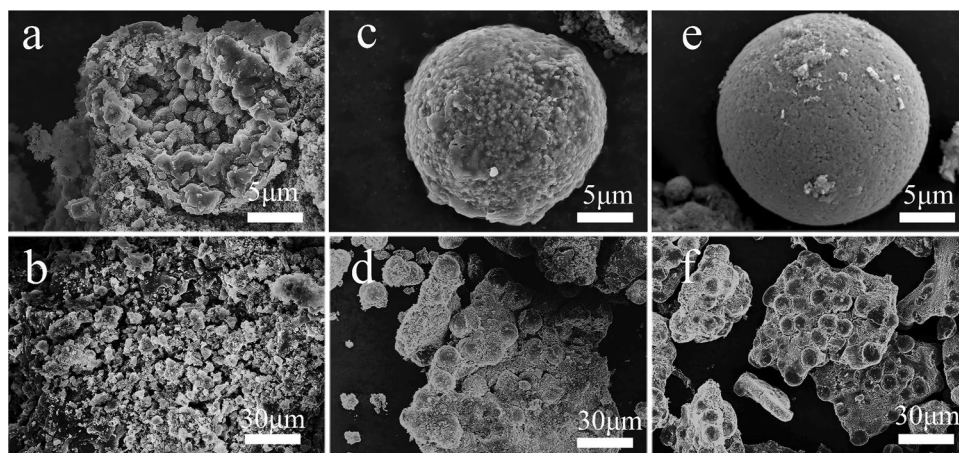
Fig. 8 NCA-Ti1.0% and NCA-NCM424Ti particle cross-section element scanning, **(a)** Ni, **(b)** Co, **(c)** Al, **(d)** Ti, **(e)** O, and **(f)** Mn



the battery was greatly enhanced. In the case of no large-scale changes in battery capacity, the highest capacity retention rates of NCA-Ti1.0% and NCA-NCM424Ti are both higher than 83%. The disadvantage of low capacity retention of nickel-rich batteries has been largely upgraded. This indicates that the modification reduces the side reactions at the interface. The enhancement of cycle

durability is mostly attributed to protecting the electrode interface and suppressing side reactions. The electrode modification mainly ameliorates the density between the crystal grains through experiments, and the electrolyte cannot easily penetrate the interface. Dense particles have better surface integrity, which enhances structural stability, and makes the particles hard to break. In summary,

Fig. 9 Cathode particles after 200 cycles, (a, b) NCA, (c, d) NCA-Ti 1.0%, and (e, f) NCA-NCM424Ti



the cycle durability of the battery is refined. The doping and coating strategies are proved to be economical and practical solutions to strengthen the cycle performance of lithium batteries.

Funding This work is financially supported by the Natural Science Foundation of Chongqing (cstc2020jcyj-msxmX0651) and the Scientific and Technological Innovation Foundation of Shunde Graduate School, USTB (grant no. BK19BE025, BK20BE012), and Research Project on Characteristic Innovation of University Teachers in Foshan City (grant no. 2020XCC04).

References

- Armand M, Tarascon J-M (2008) Building better batteries. *Nature* 451:652–657
- Yoon CS, Park K-J, Kim U-H et al (2017) High-energy Ni-rich $\text{Li}[\text{Ni}_x\text{Co}_y\text{M}_{1-x-y}]\text{O}_2$ cathodes via compositional partitioning for next-generation electric vehicles. *Chem Mater* 29:10436–10445
- Kim J, Lee H, Cha H et al (2018) Prospect and reality of Ni-Rich cathode for commercialization. *Adv Energy Mater* 8:1702028
- Zuo Y, Li B, Jiang N et al (2018) A high-capacity O_2 -type Li-rich cathode material with a single-layer Li_2MnO_3 superstructure. *Adv Mater* 30:1707255
- Kraytsberg A, Ein-Eli Y (2012) Higher, stronger, better... a review of 5 Volt cathode materials for advanced lithium-ion batteries. *Adv Energy Mater* 2:922–939
- Xia S, Li F, Cheng F et al (2018) Synthesis of spherical fluorine modified gradient Li-ion battery cathode material $\text{LiNi}_{0.80}\text{Co}_{0.15}\text{Al}_{0.05}\text{O}_2$ by simple solid phase method. *J Electrochem Soc* 165:A1019
- Zhu L, Liu Y, Wu W et al (2015) Surface fluorinated $\text{LiNi}_{0.8}\text{Co}_{0.15}\text{Al}_{0.05}\text{O}_2$ as a positive electrode material for lithium ion batteries. *J Mater Chem A* 3:15156–15162
- Ge W, Wang H, Xie Z et al (2017) Amorphous $0.035\text{Li}_2\text{O-BPO}_4$ coating for enhanced electrochemical performance of $\text{Li}[\text{Ni}_{0.5}\text{Co}_{0.2}\text{Mn}_{0.3}]\text{O}_2$ cathode material. *J Alloys Compd* 693:606–614
- Zhang Y, Wang C-Y (2009) Cycle-life characterization of automotive lithium-ion batteries with LiNiO_2 cathode. *J Electrochem Soc* 156:A527
- Huang B, Wang M, Zhao Z et al (2019) Effects of the strong oxidant treatment of precursor on the electrochemical properties of $\text{LiNi}_{0.8}\text{Mn}_{0.1}\text{Co}_{0.1}\text{O}_2$ for lithium-ion batteries. *J Alloys Compd* 810:151800
- Eom J, Kim MG, Cho J (2008) Storage characteristics of $\text{LiNi}_{0.8}\text{Co}_{0.1+x}\text{Mn}_{0.1-x}\text{O}_2$ ($x=0, 0.03, \text{ and } 0.06$) cathode materials for lithium batteries. *J Electrochem Soc* 155:A239
- Kim Y, Cho J (2007) Lithium-reactive $\text{Co}_3(\text{PO}_4)_2$ nanoparticle coating on high-capacity $\text{LiNi}_{0.8}\text{Co}_{0.16}\text{Al}_{0.04}\text{O}_2$ cathode material for lithium rechargeable batteries. *J Electrochem Soc* 154:A495
- Li D, Peng Z, Guo W, Zhou Y (2008) Synthesis and characterization of $\text{LiNi}_{0.9}\text{Co}_{0.1}\text{O}_2$ for lithium batteries by a novel method. *J Alloys Compd* 457:L1–L5
- Shi X, Wang C, Ma X, Sun J (2009) Synthesis and electrochemical properties of $\text{LiNi}_{0.9}\text{Co}_{0.1}\text{O}_2$ cathode material for lithium secondary battery. *Mater Chem Phys* 113:780–783
- Jiang D, Zhao L, Shao Y, Wang D (2015) Preparation and characterization of layered $\text{LiNi}_{0.9}\text{Co}_{0.05}\text{Mn}_{0.025}\text{Mg}_{0.025}\text{O}_2$ cathode material by a sol–gel method for lithium-ion batteries. *RSC Adv* 5:40779–40784
- Cho Y, Lee Y-S, Park S-A et al (2010) $\text{LiNi}_{0.8}\text{Co}_{0.15}\text{Al}_{0.05}\text{O}_2$ cathode materials prepared by TiO_2 nanoparticle coatings on $\text{Ni}_{0.8}\text{Co}_{0.15}\text{Al}_{0.05}(\text{OH})_2$ precursors. *Electrochim Acta* 56:333–339
- Zhou P, Zhang Z, Meng H et al (2016) SiO_2 -coated $\text{LiNi}_{0.915}\text{Co}_{0.075}\text{Al}_{0.01}\text{O}_2$ cathode material for rechargeable Li-ion batteries. *Nanoscale* 8:19263–19269
- Liu BS, Sui XL, Zhang SH et al (2018) Investigation on electrochemical performance of $\text{LiNi}_{0.8}\text{Co}_{0.15}\text{Al}_{0.05}\text{O}_2$ coated by heterogeneous layer of TiO_2 . *J Alloys Compd* 739:961–971
- Kim J-Y, Kim SH, Kim DH et al (2017) Electronic structural studies on the improved thermal stability of $\text{Li}(\text{Ni}_{0.8}\text{Co}_{0.15}\text{Al}_{0.05})\text{O}_2$ by ZrO_2 coating for lithium ion batteries. *J Appl Electrochem* 47:565–572
- Huang YQ, Huang YH, Hu XL (2017) Enhanced electrochemical performance of $\text{LiNi}_{0.8}\text{Co}_{0.15}\text{Al}_{0.05}\text{O}_2$ by nanoscale surface modification with Co_3O_4 . *Electrochim Acta* 231:294–299
- Jamil S, Ran Q, Yang L et al (2021) Improved high-voltage performance of $\text{LiNi}_{0.87}\text{Co}_{0.1}\text{Al}_{0.03}\text{O}_2$ by Li^+ -conductor coating. *Chem Eng J* 407:126442
- Shang S, Wang X, Jiang F (2021) Effects of Li_2O_2 on structure and electrochemical properties of $\text{LiNi}_{0.88}\text{Co}_{0.09}\text{Al}_{0.03}\text{O}_2$ cathode materials. *J Alloys Compd* 860:158262

23. Feng D, Liu Q, Zeng T (2021) Boosting cyclability performance of the $\text{LiNi}_{0.8}\text{Co}_{0.15}\text{Al}_{0.05}\text{O}_2$ cathode by a polyacrylonitrile-induced conductive carbon surface coating. *Ceramics International* 47:12706–12715
24. Xu Y, Li X, Wang Z et al (2015) Structure and electrochemical performance of TiO_2 -coated $\text{LiNi}_{0.80}\text{Co}_{0.15}\text{Al}_{0.05}\text{O}_2$ cathode material. *Materials Letters* 143:151–154
25. He H, Dong J, Zhang D, Chang C (2020) Effect of Nb doping on the behavior of NCA cathode: Enhanced electrochemical performances from improved lattice stability towards 4.5 V application. *Ceram Int* 46:24564–24574
26. Chen T, Li X, Wang H et al (2018) The effect of gradient boracic polyanion-doping on structure, morphology, and cycling performance of Ni-rich $\text{LiNi}_{0.8}\text{Co}_{0.15}\text{Al}_{0.05}\text{O}_2$ cathode material. *J Power Sources* 374:1–11
27. He S, Wei A, Li W et al (2019) An in-depth analysis detailing the structural and electrochemical properties within Br^- -modified $\text{LiNi}_{0.815}\text{Co}_{0.15}\text{Al}_{0.035}\text{O}_2$ (NCA) cathode material. *Electrochim Acta* 318:362–373
28. Yang H, Wu HH, Ge M et al (2019) Simultaneously dual modification of ni-rich layered oxide cathode for high-energy lithium-ion batteries. *Adv Func Mater* 29:1808825
29. Nam GW, Park N-Y, Park K-J et al (2019) Capacity fading of Ni-rich NCA cathodes: effect of microcracking extent. *ACS Energy Lett* 4:2995–3001
30. Park KJ, Choi MJ, Maglia F et al (2018) High-capacity concentration gradient $\text{Li}[\text{Ni}_{0.865}\text{Co}_{0.120}\text{Al}_{0.015}]\text{O}_2$ cathode for lithium-ion batteries. *Adv Energy Mater* 8:1703612
31. Kim UH, Ryu HH, Kim JH et al (2019) Microstructure-controlled Ni-rich cathode material by microscale compositional partition for next-generation electric vehicles. *Adv Energy Mater* 9:1803902
32. Qian K, Huang B, Liu Y et al (2019) Increase and discretization of the energy barrier for individual $\text{LiNi}_x\text{Co}_y\text{Mn}_z\text{O}_2$ ($x+2y=1$) particles with the growth of a Li_2CO_3 surface film. *J Mater Chem A* 7:12723–12731
33. Uygur CS, Aydinol MK (2021) Effect of calcium or yttrium doping on cation ordering and electrochemical performance of $\text{Li}(\text{Ni}_{0.80-x}\text{Co}_{0.15}\text{Al}_{0.05}\text{M}_x)\text{O}_2$ ($\text{M} = \text{Ca}, \text{Y}$) as a Li-ion battery cathode. *Materials Science and Engineering: B* 264:114925
34. Yu H, Li Y, Hu Y et al (2019) Concurrently coating and doping high-valence vanadium in Ni-rich lithiated oxides for high-rate and stable Li-ion batteries. *Ind Eng Chem Res* 58:4108–4115
35. Chen Z, Kim GT, Bresser D et al (2018) MnPO_4 -Coated Li-NCM: MnPO_4 -coated $\text{Li}(\text{Ni}_{0.4}\text{Co}_{0.2}\text{Mn}_{0.4})\text{O}_2$ for Lithium(-Ion) batteries with outstanding cycling stability and enhanced lithiation kinetics. *Adv Energy Mater* 8:1870123
36. Wu F, Liu N, Chen L et al (2019) Improving the reversibility of the H2-H3 phase transitions for layered Ni-rich oxide cathode towards retarded structural transition and enhanced cycle stability. *Nano Energy* 59:50–57
37. Shan W, Huang S, Zhang H, Hou X (2020) Surface coating for high-nickel cathode materials to achieve excellent cycle performance at elevated temperatures. *J Alloys Compd* 862:158022
38. Ryu H-H, Park K-J, Yoon CS, Sun Y-K (2018) Capacity fading of Ni-rich $\text{Li}[\text{Ni}_x\text{Co}_y\text{M}_{1-x-y}]\text{O}_2$ ($0.6 \leq x \leq 0.95$) cathodes for high-energy-density lithium-ion batteries: bulk or surface degradation? *Chem Mater* 30:1155–1163
39. Yoon CS, Jun DW, Myung ST, Sun YK (2017) Structural stability of LiNiO_2 cycled above 4.2 V. *ACS Energy Lett* 2:1150–1155
40. Kondrakov AO, Schmidt A, Xu J et al (2017) Anisotropic lattice strain and mechanical degradation of high and low nickel NCM cathode materials for Li-ion batteries. *J Phys Chem C* 121:3286–3294
41. Ryu HH, Park NY, Seo JH et al (2020) A highly stabilized Ni-rich NCA cathode for high-energy lithium-ion batteries. *Mater Today* 36:73–82. <https://doi.org/10.1016/j.mattod.2020.01.019>
42. Chen J, Wang XL, Jin EM et al (2021) Optimization of B_2O_3 coating process for NCA cathodes to achieve long-term stability for application in lithium ion batteries. *Energy* 222:119913
43. Takanashi S, Abe Y (2017) Improvement of the electrochemical performance of an NCA positive-electrode material of lithium ion battery by forming an Al-rich surface layer. *Ceram Int* 43:9246–9252
44. Cheng X, Liu M, Yin J et al (2020) Regulating surface and grain-boundary structures of Ni-Rich layered cathodes for ultrahigh cycle stability. *Small* 16:1906433
45. Hu X, Qiang W, Huang B (2017) Surface layer design of cathode materials based on mechanical stability towards long cycle life for lithium secondary batteries. *Energy Storage Mater* 8:141–146
46. Han Y, Cheng X, Zhao G et al (2021) Effects of Al doping on the electrochemical performances of $\text{LiNi}_{0.83}\text{Co}_{0.12}\text{Mn}_{0.05}\text{O}_2$ prepared by coprecipitation. *Ceram Int* 47:12104–12110

Publisher's note Springer Nature remains neutral with regard to jurisdictional claims in published maps and institutional affiliations.